Operando hard X-ray photoelectron spectroscopy study of the Pt/Ru/PbZr_0.52Ti_0.48O_3 interface

Ibrahima Gueye, Gwenael Le Rhun, Olivier Renault, David Cooper, Denis Ceolin, Jean-Pascal Rueff, Nicholas Barrett

▶ **To cite this version:**

Ibrahima Gueye, Gwenael Le Rhun, Olivier Renault, David Cooper, Denis Ceolin, et al.. Operando hard X-ray photoelectron spectroscopy study of the Pt/Ru/PbZr_0.52Ti_0.48O_3 interface. Applied Physics Letters, 2017, 111, pp.32906. 10.1063/1.4993909 . cea-01591616

HAL Id: cea-01591616
https://cea.hal.science/cea-01591616

Submitted on 21 Sep 2017

HAL is a multi-disciplinary open access archive for the deposit and dissemination of scientific research documents, whether they are published or not. The documents may come from teaching and research institutions in France or abroad, or from public or private research centers.

L'archive ouverte pluridisciplinaire **HAL**, est destinée au dépôt et à la diffusion de documents scientifiques de niveau recherche, publiés ou non, émanant des établissements d'enseignement et de recherche français ou étrangers, des laboratoires publics ou privés.

Operando hard X-ray photoelectron spectroscopy study of the Pt/Ru/$PbZr_{0.52}Ti_{0.48}O_3$ interface

Ibrahima Gueye,[1,2] Gwenael Le Rhun,[1,2] Olivier Renault,[1,2] David Cooper,[1,2] Denis Ceolin,[3] Jean-Pascal Rueff,[3] and Nicholas Barrett[4]
[1]*Univ. Grenoble Alpes, F-38000 Grenoble France*
[2]*CEA, LETI, MINATEC Campus, F-38054 Grenoble, France*
[3]*Synchrotron-SOLEIL, BP 48, Saint-Aubin, F-91192 Gif-sur-Yvette Cedex, France*
[4]*SPEC, CEA, CNRS, Université Paris Saclay, F-91191 Gif-sur-Yvette, France*

(Received 4 May 2017; accepted 1 July 2017; published online 19 July 2017)

We have used hard X-ray photoelectron spectroscopy to probe the Pt/Ru/$PbZr_{0.52}Ti_{0.48}O_3$ (PZT) interface in a Pt/Ru/PZT(220 nm)/Pt/TiO_2/SiO_2/Si stack. A customized sample-holder allows *in-situ* photoemission analysis while applying bias to the capacitor. Hard X-rays probe the buried interface between the top electrode and the ferroelectric PZT. The use of *operando* conditions reveals a polarization-dependent electronic response, most probably due to imperfect screening of the depolarizing field. There is evidence for an additional core level component related to the electrode-PZT interface. Zr oxide nanostructures at the surface of the sol-gel layer may form a ferroelectric dead layer at the interface, affecting device performance. *Published by AIP Publishing.*
[http://dx.doi.org/10.1063/1.4993909]

Ferroelectric $Pb(Zr,Ti)O_3$ (PZT) thin films are envisaged in the new generation of decoupling multiple metal-insulator-metal (MIM) stacks showing enhanced capacitance density and breakdown voltage.[1] Sol-gel is a method of choice for the growth of PZT films.[2] Indeed, 200 nm PZT capacitors have demonstrated a permittivity of 900, a capacitance density of 40 nF/mm^2, and a breakdown voltage of 30 V.[3] However, the electrode/PZT interface can play a key role in polarization switching, permittivity, breakdown voltage, fatigue, and reliability.[4–6] The Schottky barrier height (SBH) has an important influence on leakage current[7] and depends on the polarization.[5,8–10] On a microscopic scale, it is determined by the local chemistry,[10,11] and the resulting interfacial layer has been described in terms of an additional capacitor in series[12] with specific, bias dependent chemistry and screening of the depolarizing field.[13]

X-ray photoelectron spectroscopy (XPS) is an ideal tool to probe changes in local chemical and electronic structures, but to investigate the material response to electrical stimulation, an experimental set-up to perform *operando* measurements, i.e., under *in-situ* bias, is required. Chen and Klein used XPS with *in-situ* bias to probe the interface between single crystal $BaTiO_3$ (BTO) and Pt or RuO_2 electrodes.[9] Rault *et al.* have measured the Pt/BTO/n-doped $SrTiO_3$ (STO) interface band line-up as a function of polarization.[8] Standard XPS is very surface sensitive and requires ultra-thin electrodes which may be discontinuous or poorly metallic. Hard X-ray Photoelectron Spectroscopy (HAXPES) allows access to more deeply buried interfaces,[14] making the study of more realistic device architectures possible. Zenkevich *et al.*[15] have measured the barrier-height at the top interface of a Pt/BTO/Cr tunnel junction after *ex situ* switching. Interestingly, it was recently shown that applied bias gives rise to an additional core level shift due to the strain generated in a relaxor ferroelectric.[10] Such an effect is absent under the zero field, underlining the importance of operando experiments for a comprehensive understanding of device operation.

Here, we combine HAXPES with *in-situ* biasing to carry out an *operando* study of the top interface chemistry and electronic structure of a Pt(5 nm)/Ru(5 nm)/PZT(220 nm)/Pt/TiO_2/SiO_2/Si capacitor as a function of saturation polarization. The results are correlated with electrical characterization, cross-sectional transmission electron microscopy (TEM), and surface chemistry of the PZT layer before electrode growth.[16]

The samples were prepared at the MINATEC High-Technologies Building and Upstream Technological Platform cleanrooms of CEA-LETI (Grenoble). Sol-gel PZT, with 10% excess Pb precursor, was grown on a Pt/TiO_2/SiO_2/Si substrate to provide a reference film. The details of the sol-gel growth are given elsewhere, and the films are strongly textured (100) as shown by X-ray diffraction.[16] The Pt(5 nm)/Ru(5 nm) top electrode was deposited using DC magnetron sputtering. The Pt/Ru electrode leads to better saturation capacitance and breakdown voltage than pure Pt since the Ru interlayer ensures better adhesion of Pt, avoiding delamination. The full layers were lithographically etched to provide easy wiring of the top and bottom electrodes. Figure 1(a) shows the high resolution bright field TEM cross-section. The crystalline Zr oxide based nanostructures already observed at the surface of bare PZT[16] are clearly present at the interface. These structures are known to appear at the surface of the sol-gel layer during synthesis due to the exhaustion of the PbO precursor before ZrO_2.[16,17] The typical nanostructure diameter is 15 nm, and the Pt-Ru electrode follows their topography. Figure 1(b) shows the Energy Dispersive X-Ray Analysis cross-sections for Pb, Zr, and O, confirming the Zr oxide composition.

The structure was biased using an Agilent E4980A capacimeter/voltage generator. The C-V characteristic at 1 kHz is offset by −1.55 V, and the coercive voltages are −2.0 and −1.2 V [Fig. 1(c)]. At the zero applied field, there is a strong, downwards pointing imprint polarization, which we will call P^-. The capacitance does not change during the long exposure to

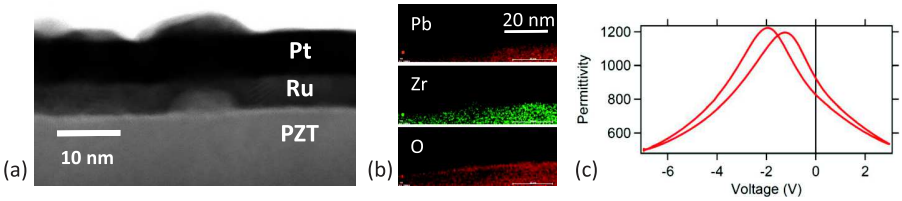

FIG. 1. (a) High-resolution bright field TEM cross-section of the as-grown Pt/Ru/PZT interface. (b) Pb, Zr, and O cross-sections of the Ru/PZT interface and (c) permittivity-voltage characteristic.

high energy X-rays. Dynamic hysteresis measurement at 1 kHz (using an Aixacct TF2000 ferroelectric tester) reveals a saturation polarization equal to 23 μC/cm^2.

The HAXPES experiments were done at the Galaxies beamline of the SOLEIL synchrotron (Saint Aubin, France) using a photon energy of 6893.6 eV as calibrated by the Fermi level of the top electrode. The photon and analyzer bandwidths were 150 meV and 180 meV, respectively, giving a total resolution of ~235 meV. Figure 2(a) shows a schematic of the sample geometry. Two sample plates are used on the manipulator, the first one for the sample mounting and top electrode bias, and the second one to contact the bottom electrode via a Cu spring contact. The *operando* analysis was carried out at −7 V (negative voltage on the top electrode, P^+ polarization) and +3 V (positive voltage on the top electrode, P^- polarization), i.e., symmetrically with respect to the center of the butterfly loop of Fig. 1(c). Remanence measurements are expected to show a similar result to +3 V since the imprint polarization is P^-. The high voltages relative to the coercive values ensure true saturation conditions whilst remaining below breakdown.

The survey spectra of the reference PZT film without the electrode and the MIM structure with the 10 nm Pt/Ru top electrode are shown in Fig. 2(b). In the latter, the characteristic PZT peaks of the reference layer are strongly attenuated with respect to the reference film, consistent with the estimated inelastic mean free path (IMFP) for Pb 4d and Zr 3s electrons excited by 6.9 keV photons (5.9 and 5.5 nm in Ru and Pt, respectively).[18] The odd looking shape of the Zr 3d emission comes from enhancement of the signal from the nanostructures due to the high IMFP.

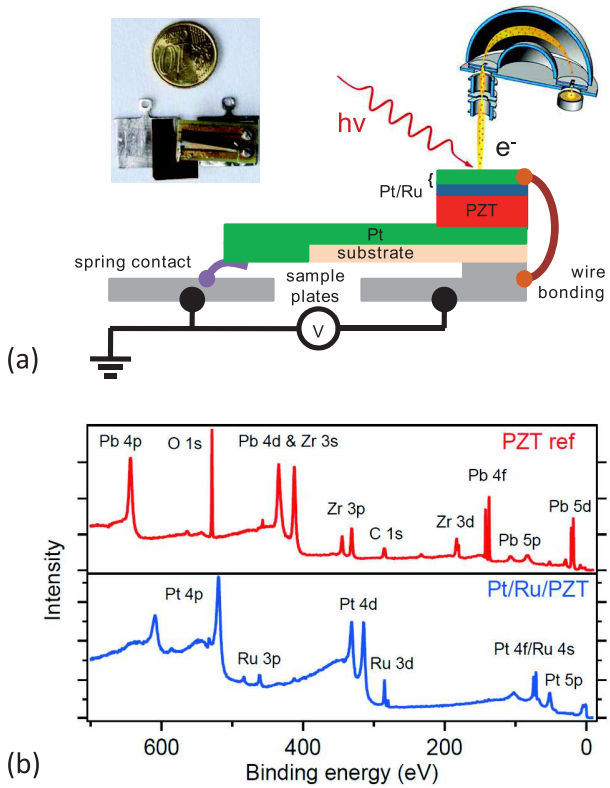

FIG. 2. (a) Sample geometry and (b) HAXPES survey spectra of the PZT reference film (top, red) and the Pt/Ru/PZT structure (bottom, blue).

In Fig. 3(a), we present the Pb 4f and Zr 3p$_{3/2}$ core level spectra of the PZT reference film, i.e., without the top electrode. The results of the fits are given in Table I. The main Pb 4f component (peak I) corresponds to Pb^{2+} in PZT. The low binding energy (LBE) component (peak II), shifted by 1.3 eV with respect to the main peak, accounts for 5% of the total intensity and represents reduced Pb, possibly as a result of exposure to the high energy X-rays, although no evolution is observed during data acquisition. This small proportion of reduced Pb may therefore be intrinsic to the sol-gel layer.

The Zr 3p$_{3/2}$ spectrum in Fig. 3(b) also has two components. The main peak (I) at 331.5 eV is the Zr emission from the PZT, whereas the peak (II) shifted 1.0 eV to higher binding energy (HBE) has been identified as being due to the $ZrO_{1.89}$ nanostructures at the PZT surface.[16] The binding energy shift is consistent with the Pauling electronegativities of Zr and Ti (1.33 and 1.45, respectively). The core level shifts and intensity ratios of the reduced/PZT Pb and nanostructure/PZT Zr in the reference film have been directly transposed to the Pb 4d/Zr 3s spectra presented below in the analysis of the *operando* spectra. Therefore, the only free parameters are the absolute binding energy, the intensity, and any additional, interface specific component.

The raw data of the Ru 3p, Pb 4d, and Zr 3s spectral regions from the capacitor structure with −7 V (red curve) and +3 V (blue) on the top electrode are shown in Fig. 4. The advantage of the Pb 4d/Zr 3s energy window is that the similar kinetic energies guarantee the same depth sensitivity, despite the additional difficulty that the Zr 3s peak partially overlaps the Pb 4d$_{3/2}$, making deconvolution more difficult.

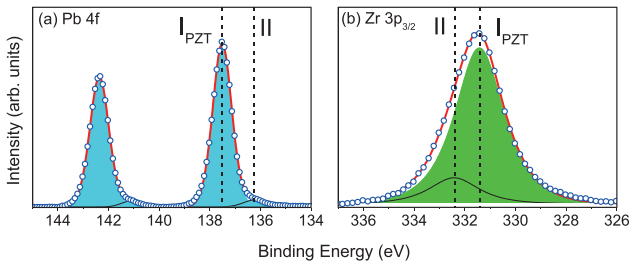

FIG. 3. (a) Pb 4f and (b) Zr 3p$_{3/2}$ spectra. The Pb components are in cyan and the Zr components are in green. The label I represents Pb/Zr in PZT, whereas label II identifies reduced Pb or Zr in surface nanostructures, respectively.

TABLE I. Core level binding energy, FWHM, and percentage of Gaussian peak in the Gaussian-Lorentzian (GL) peak shapes of the PZT reference spectra.

	Binding energy (eV)			
	I	II	FWHM (eV)	GL (%)
Pb $4f_{7/2}$	137.5	136.2	0.89	30
Zr $3p_{3/2}$	331.4	332.4	2.3	80
Pb $4d_{5/2}$	412.5	411.2	3.6	82
Zr 3s	432.0	433.0	6.0	70

The Ru 3p peak in the two bias states is separated by 10 eV, showing that there is very little parasitic resistance in the circuit. Once corrected for bias, the spectra are similar (see Fig. 4, bottom) and the residual differences can be attributed to polarization-dependent changes. The Ru $3p_{3/2}$ spectrum (not shown) has only a single component (at 461.5 eV) for both bias states, confirming an unoxidized electrode with a sharp interface, as observed in bright field TEM image of Fig. 1(a).

Due to the energy loss tail of the Pt 4d emission from the top electrode, the background actually increases with kinetic energy in the Pb 4d/Zr 3s region and standard background subtraction cannot be used. We have tested polynomial and linear backgrounds and found that the latter gives better results.

Figure 5 shows the best fits to the Pb 4d/Zr 3s spectrum for (a) the reference film and (b)–(d) the *operando* spectra with the top electrode under bias. The binding energies are given in Table II.

The reference spectrum has a high signal to noise ratio which is to be expected in the absence of attenuation by the 10 nm Pt/Ru top electrode observed on the capacitor structures. For the spectra with the top electrode under bias, once the PZT Pb 4d and PZT Zr 3s reduced Pb and Zr oxide nanostructure components have been included, there remain two important differences with respect to the reference film.

First, there is a 1.4 eV systematic shift of both Pb and Zr emission to HBE going from +3 V (P^-) to −7 V (P^+)

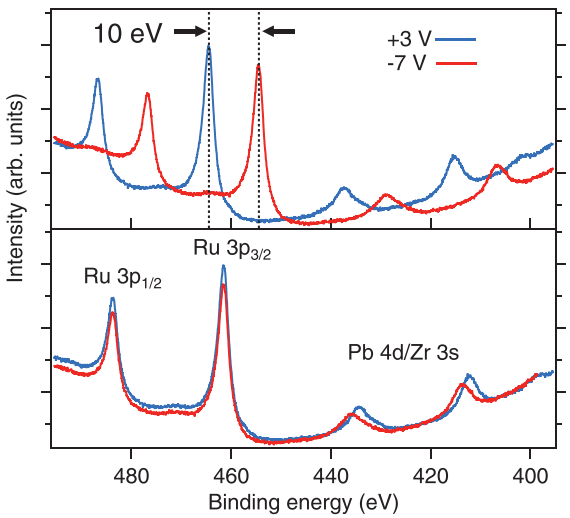

FIG. 4. (Top) *Operando* Ru 3p, Pb 4d, and Zr 3s spectra with −7 (red curve) and +3 V (blue) on the top electrode before (top) and after (bottom) correction for bias.

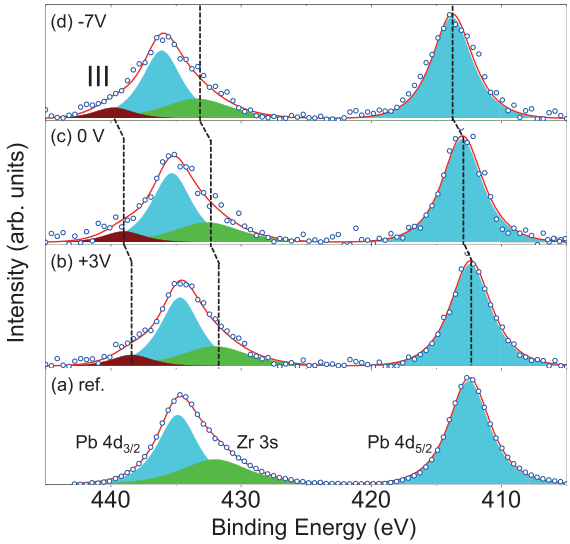

FIG. 5. Pb 4d and Zr 3s spectra and best fits for (a) reference film without electrode compared to that with the electrode under (b) +3 (c) 0 and (d) −7 V applied bias. The Pb and Zr components have been transposed from the reference spectra and the color code is the same as in Fig. 3. Label III identifies the interface related peak discussed in the text.

whereas the Ru core level *does not shift* (as shown in Fig. 4). This suggests a change in electrostatic boundary conditions rather than the chemical environment since the latter would also affect the first layer or layers of the Ru electrode. The core level shift between +3.0 and 0.0 V is smaller than between 0 V and −7.0 V consistent with the P^- imprint measured electrically. Assuming that the polarization-dependent core level shift is equal to the potential drop across the film, then the residual internal field is 65 kV/cm, approximately three times the coercive field demonstrating that the polarization charge is poorly screened. We note that the Zr 3s component due to the nanostructures is fixed since the nanostructures are above the PZT layer and should therefore be independent of the polarization; however, the nanostructures might show polarization due to stray fields, which remains an open question.

Second, there is an additional component, labelled peak III at high binding energy (439 eV). The single component suggests that it is due to Zr 3s; however, 5–6 eV is too big to be a simple chemical shift of Zr which is already in the Zr^{4+} valence state in PZT. The absence of such a component in the reference spectrum and in the XPS analysis of the bare PZT layer[16] proves that it is related to the capacitor structure; however, the cross-sectional TEM shows no evidence of an additional phase at the interface. In the fits shown in Figs. 5(b)–5(d), the component shifts from 439.8 eV at −7 V bias to 438.4 eV at +3 V bias, but it was also possible to fix the binding energy at 439 eV, which would correspond to a pure

TABLE II. Pb $4d_{5/2}$ and Zr 3s core level binding energies (eV) as a function of applied bias on the top electrode of the PZT capacitor.

	Bias on the top electrode (V)		
	+3.0	0.0	−7.0
Pb $4d_{5/2}$	412.4	413.0	413.8
Zr 3s	432.0	432.6	433.4

interface contribution, distinct from the PZT. The exact origin of this component is therefore not clear.

One possibility is interface rumpling. The intensity is 4.7% of the total. Assuming an IMFP of 5.7 nm (average of values in Ru and Pt), the intensity corresponds to that expected from a 1–2 unit cell layer of PZT. First principles calculations have shown that rumpling at the electrode interface changes significantly with polarization.[12] This has to be confirmed by further experiments with higher statistics and by acquiring the Pb 4f and Zr 3p.

The valence band offset at the interface is calculated using the following expression of binding energies: Ru $3p_{3/2}$-(Ru $3p_{3/2}$-Pb $4d_{5/2}$)–(Pb $4d_{5/2}$-VBM),[19] where the last term is measured on the PZT reference film without the top electrode and VBM is the valence band maximum. The resulting offset is $2.1(0.7) \pm 0.1$ eV for $-7(+3)$ V applied bias. Assuming a 3.4 eV band gap, this gives a SBH for electrons of $1.3(2.7) \pm 0.1$ eV, consistent with the capacitive behavior in Fig. 1(c). From the difference in SBH, we can also estimate the effective screening length using $\Delta\phi = 2\lambda_{\text{eff.}}D_S/\epsilon_0$ to be 0.23 ± 0.02 Å, in quite good agreement with the above-mentioned first principles calculations for the Pt-$PbTiO_3$ interface of 0.11 Å.[12,20]

We consider the Zr oxide nanostructures as a continuous layer to be modeled as a series capacitor. A 226 nm PZT layer with a dielectric constant of 900 in series with a 15 nm ZrO_2 layer with a dielectric constant of 25 (Ref. 21) has a total capacitance 4 times smaller than the PZT layer. In our case, the nanostructures cover approximately 1/5th of the surface; one can estimate a twofold reduction in the effective capacitance. The presence of such a dielectric layer may explain the poor screening and hence a high internal field estimated from the core level shifts. A further contribution to the poor screening may also be the relatively thin top electrode (10 nm), although a clear Fermi edge is observed in the photoemission spectra.

In conclusion, we have carried out *operando* hard X-ray photoelectron spectroscopy of the top interface in a Pt/Ru/PZT(220 nm)/Pt/TiO_2/SiO_2/Si capacitor structure. *Operando* analysis highlights several important results. Screening of the depolarizing field is bias dependent. $ZrO_{1.89}$ nanostructures present at the surface of the bare sol-gel film act as a dead layer in the capacitance structure and reduce screening. The Schottky barrier height for electrons is 1.3 and 2.7 eV for upwards and downwards pointing polarization, respectively, consistent with the electrical characteristics, and the effective screening length, as calculated from the difference in SBH, is 0.23 ± 0.02 Å. More work is required to fully characterize the origin of the HBE peak in the Pb 4d and Zr 3s spectra and the possible consequences in terms of an interface dielectric response.

The results show that an optimization of the PZT surface via elimination of the parasitic $ZrO_{1.89}$ phase would be needed to improve the interfacial dielectric response in view of an optimal use in ferroelectric capacitor application. The methodology could be adapted to *operando* studies of active devices, for example, gate/channel interfaces in transistors based on functional oxides.

The authors thank Hervé Denis for preliminary TEM/EDX measurements. We acknowledge SOLEIL for provision of synchrotron radiation facilities.

[1]M. Klee, H. Boots, B. Kumar, C. V. Heesch, R. Mauczok, W. Keur, M. D. Wild, H. V. Esch, a. L. Roest, K. Reimann, L. V. Leuken, O. Wunnicke, J. Zhao, G. Schmitz, M. Mienkina, M. Mleczko, and M. Tiggelman, IOP Conf. Ser.: Mater. Sci. Eng. **8**, 012008 (2010).
[2]F. Calame and P. Muralt, Appl. Phys. Lett. **90**, 062907 (2007).
[3]P. Belleville, J. Bigarre, P. Boy, and Y. Montouillout, J. Sol-Gel Sci. Technol. **43**, 213 (2007).
[4]J. F. Scott, *Ferroelectric Memories* (Springer-Verlag, Berlin, Heidelberg, 2000).
[5]F. Chen, R. Schafranek, A. Wachau, S. Zhukov, J. Glaum, T. Granzow, H. von Seggern, and A. Klein, J. Appl. Phys. **108**, 104106 (2010).
[6]X. J. Lou, J. Appl. Phys. **105**, 024101 (2009).
[7]L. Pintilie and M. Alexe, J. Appl. Phys. **98**, 124103 (2005)..
[8]J. E. Rault, G. Agnus, T. Maroutian, V. Pillard, P. Lecoeur, G. Niu, B. Vilquin, M. G. Silly, A. Bendounan, F. Sirotti, and N. Barrett, Phys. Rev. B **87**, 155146 (2013).
[9]F. Chen and A. Klein, Phys. Rev. B **86**, 094105 (2012).
[10]E. Kröger, A. Petraru, A. Quer, R. Soni, M. Kalläne, N. a. Pertsev, H. Kohlstedt, and K. Rossnagel, Phys. Rev. B - Condens. Matter Mater. Phys. **93**, 235415 (2016).
[11]I. Pintilie, C. M. Teodorescu, C. Ghica, C. Chirila, A. G. Boni, L. Hrib, I. Pasuk, R. Negrea, N. Apostol, and L. Pintilie, ACS Appl. Mater. Interfaces **6**, 2929 (2014).
[12]Y. Kim, C. Bae, K. Ryu, H. Ko, Y. K. Kim, S. Hong, and H. Shin, Nat. Mater. **8**, 392 (2009).
[13]P. Zubko, J. C. Wojde, M. Hadjimichael, S. Fernandez-Pena, A. Sené, I. Lukyanchuk, J.-M. Triscone, and J. Íñiguez, Nature **534**, 524 (2016).
[14]C. S. Fadley, J. Electron Spectrosc. Relat. Phenom. **178–179**, 2 (2010).
[15]A. Zenkevich, Y. Matveyev, M. Minnekaev, Y. Lebedinskii, S. Thiess, and W. Drube, J. Electron Spectrosc. Relat. Phenom. **190**, 302 (2013).
[16]I. Gueye, G. Le Rhun, P. Gergaud, O. Renault, E. Defay, and N. Barrett, Appl. Surf. Sci. **363**, 21 (2016).
[17]A. Zomorrodian, A. Mesarwi, N. J. Wu, and A. Ignatiev, Appl. Surf. Sci. **90**(3), 343 (1995).
[18]H. Shinotsuka, S. Tanuma, C. J. Powell, and D. R. Penn, Surf. Interface Anal. **47**, 871 (2015).
[19]E. A. Kraut, R. W. Grant, J. R. Waldrop, and S. P. Kowalczyk, Phys. Rev. Lett. **44**, 1620 (1980).
[20]M. Stengel, P. Aguado-Puente, N. Spaldin, and J. Junquera, Phys. Rev. B **83**, 235112 (2011).
[21]D. Vanderbilt, X. Zhao, and D. Ceresoli, Thin Solid Films **486**, 125 (2005); e-print arXiv:0606340 [cond-mat].